Rapidity dependence of deuteron production in Au+Au collisions at $\sqrt{s_{\rm NN}}$= 200 GeV

I. Arsene,[11,*] I. G. Bearden,[5] D. Beavis,[1] S. Bekele,[10,†] C. Besliu,[9] B. Budick,[3] H. Bøggild,[5] C. Chasman,[1] C. H. Christensen,[5] P. Christensen,[5,‡] H. H. Dalsgaard,[5] R. Debbe,[1] J. J. Gaardhøje,[5] C. E. Jørgensen,[5,§] K. Hagel,[7] H. Ito,[1] A. Jipa,[9] E. B. Johnson,[10,¶] R. Karabowicz,[4] N. Katrynska,[4] E. J. Kim,[10,**] T. M. Larsen,[5] J. H. Lee,[1] G. Løvhøiden,[11] Z. Majka,[4] M. Murray,[10] J. Natowitz,[7] B. S. Nielsen,[5] C. Nygaard,[5] D. Ouerdane,[5] D. Pal,[10] A. Qviller,[11] F. Rami,[2] C. Ristea,[5] O. Ristea,[9] D. Röhrich,[8] S. J. Sanders,[10] P. Staszel,[4] T. S. Tveter,[11] F. Videbæk,[1,††] R. Wada,[7] H. Yang,[8,‡‡] Z. Yin,[8,§§] and S.Zgura[6]

(The BRAHMS Collaboration)

[1]*Brookhaven National Laboratory, Upton, NY 11973-5000, U.S.*
[2]*Institute Pluridisciplinaire Hubert Curien CRNS-IN2P3 et Université de Strasbourg, Strasbourg, France*
[3] *New York University, New York, NY 10003*
[4] *Smoluchowski Inst. of Physics, Jagiellonian University, Krakow, Poland*
[5]*Niels Bohr Institute, Blegdamsvej 17, University of Copenhagen, Copenhagen 2100, Denmark*
[6]*Institute for Space Sciences, Bucharest, Romania*
[7]*Texas A&M University, College Station, TX 17843*
[8] *University of Bergen, Department of Physics and Technology, Bergen, Norway*
[9] *University of Bucharest, Bucharest, Romania*
[10]*University of Kansas, Lawrence, KS 66045*
[11]*University of Oslo, Department of Physics, Oslo, Norway*

(Dated: April 14, 2010)

We have measured the distributions of (anti)-protons and (anti)-deuterons produced in high energy heavy ion Au+Au collisions at RHIC over a very wide range of transverse and longitudinal momentum. We present our results in the context of coalescence models. In particular we extract the "volume of homogeneity" and the average phase-space density for protons and anti-protons. Near central rapidity the coalescence parameter $B_2(p_T)$ and the space averaged phase-space density $f(\rm p_T)$ are very similar for both protons and anti-protons. For protons we see little variation of either $B_2(\rm p_T)$ or the space averaged phase-space density as the rapidity increases from 0 to 3.1. However both these quantities depend strongly on p_T at all rapidities. These results are in contrast to lower energy data where the proton and anti-proton phase space densities are different at y=0 and both B_2 and f depend strongly on rapidity.

PACS numbers: 25.75.Gz, 25.75.Ld, 13.85.2t, 25.40.Ve

I. INTRODUCTION

Deuterons detected in heavy ion collisions are conventionally thought to be produced via a process called coalescence. Nucleons that are close enough in phase space, i.e. in position and momentum space "coalesce" to form deuterons. In free space, such a reaction would be $p + n \rightarrow d + \gamma$; while in a heavy-ion collision the surrounding hot and dense medium ensure energy and momentum conservation. As the clusters are formed inside the expanding system created in the A+A collisions, they continue to interact and may be broken up back into nucleons. These competing mechanisms last until the later stages of the expansion. Due to its low binding energy, the detected deuterons are most likely formed very near freeze-out and are thus considered an ideal probe to the latest space-time properties of the system.

Coalescence models assume that the distribution of clusters is just proportional to the product of the distributions of individual nucleons [1–3]. For deuterons this is written as

$$E_d \cdot \frac{d^3N_d}{dp_d^3} = B_2(E_p \cdot \frac{d^3N_p}{dp_p^3})^2, \qquad (1)$$

where it is assumed that the unmeasured neutron spectra are identical to the measured proton spectra and that the momentum of the deuteron is trivially the sum of the nucleon momenta. Note that at $\sqrt{s_{\rm NN}}$= 4.9 GeV the measured n/p ratio has a value of $1.19 \pm .08$ and is independent of m_T [4]. In models that assume thermalized

*Present Address: ExtreMe Matter Institute EMMI, GSI Helmholtzzentrum für Schwerionenforschung GmbH,Darmstadt, Germany
†Present address: Dept of Physics, Tennessee Tech University,Cookeville, Tennessee
‡Present Address: Div. of Experimental High-Energy Physics, Lund University, Lund, Sweden
§Present address: Risø National Laboratory, Denmark
¶Present Address: Radiation Monitoring Devices, Cambridge, MA, USA
**Present address: Division of Science Education, Chonbuk National University, Jeonju, 561-756, Korea
††Spokesperson
‡‡Present Address: Physics Institute, University of Heidelberg, Heidelberg, Germany
§§Present address: Institute of Particle Physics, Huazhong Normal University,Wuhan,China

distributions of nucleons, B_2 carries information about the cluster since it is inversely proportional to the volume of the system in coordinate space [1–3]. For low and intermediate energy heavy ion collisions and high energy pA collisions, the measured B_2 is independent of energy and p_T and is consistent with measurements of the deuteron wave-function [5]. At higher energies, $\sqrt{s_{\rm NN}} \geq$ 4.9 GeV, B_2 decreases with energy and increases with p_T [6–10]. This is consistent with the formation of deuterons in an expanding medium [11–13]. The connection of B_2 to coordinate space is highlighted in coalescence models that use the so called Wigner functions to write the yield of clusters as convolutions of nucleon distributions in momentum and space-time and the deuteron wave function as the coalescence function. Approximating the deuteron wave function by a Gaussian distribution, and assuming that the region where coalescence occurs has also a Gaussian shape with width R_G [14], one can write:

$$(R_G^2 + \frac{\delta^2}{2})^{3/2} = \frac{3}{2} \cdot \frac{\pi^{3/2}\hbar^3}{B_2 \cdot m_p c^2}, \tag{2}$$

where m_p denotes the proton mass. The δ parameter accounts for the size of the deuteron and has a value of δ = 2.8 fm. One advantage of this ansatz is that it facilitates comparison to interferometry radii. The deuteron wave-function is more accurately represented by the Hulthen form, which has an exponential tail [15]. For the B_2 values reported in this paper the error in R_G from using Eq. 2 is less than 0.2 fm [16]. Near mid-rapidity B_2 decreases with energy up to $\sqrt{s_{\rm NN}}$= 17.3 GeV [19] before flattening out at RHIC energies [20, 21]. This is similar to the behavior seen in HBT radii [22].

However, it has been suggested that for a strongly interacting plasma of quarks and gluons deuterons may be formed by direct coalescence of quarks. It should be noted that for central rapidity and deuteron $p_T > 1.5$ GeV/c the elliptic flow per quark for deuterons scales as $\rm p_T/n_{quark}$ just as it does for lighter hadrons [6]. Within the AMPT model calculations based on the direct production of deuterons are closer to the flow data than calculations based on nucleon coalescence [23]. However the authors note that including the hadronic re-scattering of deuterons may change this conclusion.

The average of the phase-space density $f(\mathbf{x}, \mathbf{p})$ over the system volume at freeze-out time is a quantity, which, when compared to Bose-Einstein or Fermi-Dirac statistics, allows the assessment of the degree of chemical or kinetic equilibrium reached by the system at that stage. This quantity also carries information about the possible multiple-particle symmetrization effects i.e. pion condensates and is related to the entropy of the system. The spatial average phase-space density is defined as the following ratio:

$$\langle f \rangle(\mathbf{p}) \equiv \frac{\int d^3x f^2(\mathbf{x}, \mathbf{p})}{\int d^3x f(\mathbf{x}, \mathbf{p})}, \tag{3}$$

where the integration is carried over spatial coordinates bound by the volume of the system at freeze-out. With the formal definition of phase-space density for a particle of spin J written as:

$$f(\mathbf{x}, \mathbf{p}) \equiv \frac{(2\pi\hbar)^3}{(2J+1)} \frac{d^6N}{dp^3dx^3}. \tag{4}$$

For a system in chemical equilibrium at a temperature T and chemical potential μ

$$f(E) = \frac{1}{e^{(E-\mu)/T} \pm 1}, \tag{5}$$

where E is the energy and ± 1 selects bosons or fermions. For a dilute system, *i.e.* $f \ll 1$, Eq. 5 gives

$$f_d \approx e^{-(E_d - \mu_p - \mu_n)/T}. \tag{6}$$

Since $E_d = m_T \cosh(\rm y)$, one would expect the phase-space density to be an exponential in m_T. Note in this simple derivation, we are ignoring the collective motion of the of particles. At $\sqrt{s_{\rm NN}}$ = 17.3 GeV, it was found that strong longitudinal flow could significantly reduce the pion phase-space density [24]. Also at this energy the inverse slope of the phase-space density was found to increase with particle mass in a manner suggestive of transverse flow [25]. Because $E_d = E_n + E_p$, Eq. 6 implies that

$$f_d(\mathbf{x}, \mathbf{P}) = f_p(\mathbf{x}, \mathbf{p}) \cdot f_n(\mathbf{x}, \mathbf{p}) = f_p(\mathbf{x}, \mathbf{p})^2. \tag{7}$$

To extract the average phase-space density of protons one can then replace the square term in the numerator of Eq. 3 by the phase-space density of deuterons:

$$\langle f_p \rangle = \frac{1}{3}(E_d \frac{d^3N_d}{dp_d^3})/(E_p \frac{d^3N_p}{dp_p^3}). \tag{8}$$

Alternatively one can make use of the assumption that deuterons are formed by coalescence and satisfy Eq. 1 to obtain an expression for the average phase space of protons similar to what Bertsch originally suggested for pions; dividing the spectrum by the product of the HBT radii [26, 27]:

$$\langle f_p \rangle = \frac{1}{2} \cdot E_p \frac{d^3N_p}{dp^3} \frac{\pi^{3/2} \cdot \hbar^3}{R_G^3 \cdot m_p c^2}. \tag{9}$$

Note this represents the maximum space averaged phase-space density, which is at the center of the Gaussian source [27]. The phase space densities calculated using Eq. 8 have the expected exponential dependence in m_T. When using Eq. 9 one introduces the assumption that deuterons are produced via coalescence and that

the homogeneity volume extracted from deuteron distributions is also the volume of the proton source. The calculation of the space averaged phase-space density of protons using these assumptions is close in value to the one obtained from an assumed thermal equilibrium and has the same behavior in m_T. This suggests that the system has evolved into chemical equilibrium at freeze-out. To ease the comparison with lower energy data we have decided to use Eq. 8 to calculate the phase density.

The coalescence parameter and the space averaged phase-space density recast the information contained in the proton and deuteron spectra into "dynamic" and "chemical" terms. The coalescence parameter B_2 can be interpreted in terms of a "radius of homogeniety," which depends upon the temperature of the system and the radial flow. Indeed one confirmation that we are actually seeing coalescence would be if the this radius was consistent with the appropriate HBT radii. This was checked at $\sqrt{s_{\rm NN}}$=17.3 GeV by comparing R_G to radii extracted from pp and $\pi\pi$ correlation measurements [16–18]. The magnitude of the space averaged phase-space density is sensitive to the chemical potential of the system while its energy dependence derives from the temperature and flow of the matter. In this paper, we use the very large angular and momentum ranges of the two BRAHMS spectrometers to measure the rapidity dependence of the size and space averaged phase-space density of the (anti)-proton distributions for central Au+Au collisions.

II. ANALYSIS

The data in this paper were collected by the BRAHMS experiment during 2004. We present proton and deuteron spectra at $\sqrt{s_{\rm NN}}$ =200 GeV AuAu collisions with a centrality range of 0-20%. The data are analysed in four rapidity bins: $(-0.1, 0.1)$, $(0.5, 1.0)$, $(1.5, 2.5)$, and $(2.8, 3.2)$.

A. Detector System

The BRAHMS experimental setup consists of two movable magnetic spectrometers, the Forward Spectrometer (FS) that can be rotated from 2.3° to 15° , and the Mid-Rapidity Spectrometer (MRS) that can be rotated from 34° to 2.3° degrees relative to the beam line, a set of global detectors consisting of silicon and scintilator tile arrays used to measure charged particles multiplicities, as well as fast Cherenkov counters at high rapidity used to measure luminosity, to determine the interaction vertex, and to provide a start time for time-of-flight measurements.

The MRS has two Time Projection Chambers (TPCs), TPM1 and TPM2, situated in field free regions in front and behind a dipole magnet. This assembly is followed by a highly segmented scintillator time-of-flight wall at 4.51 m. The FS consists of 4 dipole magnets D1, D2, D3 and D4 with a total bending power of up to 9.2 Tm. The spectrometer has 5 tracking stations T1 through T5. T1 and T2 are TPCs placed in front of and after the second dipole D2. T3, T4 and T5 are drift chambers with T3 in front of D3, T4 between D3 and D4, and T5 after D4 and just in front of the Ring Imaging Cherenkov (RICH) [28]. Details on the BRAHMS experimental setup can be found in Ref. [29] and in Ref. [30] for tracking in the MRS.

B. Tracking

Local tracks are first determined in the TPCs and Drift Chambers, which are situated in field free region. The resulting straight-line track segments in two tracking chambers located on either side of a magnet are matched using the effective edge approximation generating matched tracks. Local tracks and local matched tracks are combined in the FS to form complete tracks. The complete tracks are refitted to deduce the final momenta. Tracks in the FS are required to project through the magnet D1 onto the nominal beamline. Track quality cuts are applied for the final track selection.

We correct our raw momentum distributions for tracking detector efficiency and geometrical acceptance. GEANT 3.21 is used to correct for absorption, multiple scattering, and energy loss in the detectors [31]. We assume that deuteron absorption factorizes from other effects and model it as the square of the proton absorption correction (at $p_T/2$) [16].

C. Particle Identification

In the midrapidity region, particle identification is done using time of flight measurements, while at forward rapidities we use the RICH. At y=0 and 0.75 we select (anti-)protons using a 3σ cut on $m^2 = p^2(\frac{c^2L^2}{t^2}-1)$, where L is the length of the path followed by a particle, t its time of flight and c the speed of light. For deuterons a simple 3σ cut around the (anti-)deuteron mean mass is used. At forward rapidities the RICH provides proton deuteron PID separation. The ring radius in the RICH depends on the particle's velocity. For a particle of mass m in our RICH $R \approx 9.2(1-(p/p_{thres})^2)$ cm where $p_{thres} = m16.1c$. The PID performance is shown in Fig. 1, where the bands represent the limits used for the analysis. Because of various inefficiencies about 3% of particles moving faster than their Cherenkov threshold don't produce a ring. Protons and deuterons with momenta between the kaon and proton thresholds do not make a ring. The contamination from mis-identified kaons and pions are subtracted to deduce the proton spectrum in this momentum range (neglecting the small fraction of deuterons). This procedure cannot be used in the region between the proton and deuteron thresholds

since the contaminations from pions, kaons and protons dominates the small deuteron yield.

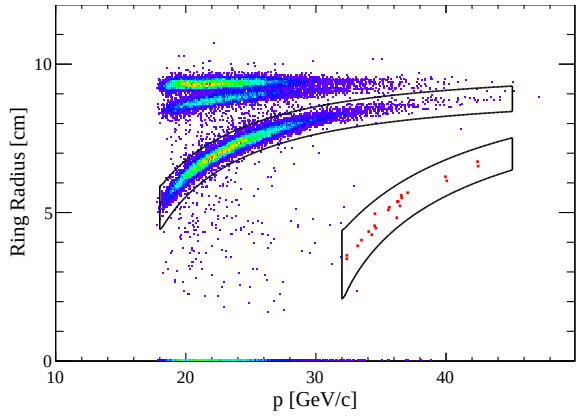

FIG. 1: (color online). Ring radius versus momentum for particles with $y \approx 3$ showing the pion, kaon, proton and deuteron separation. The bands show the protons and deuterons used in the analysis.

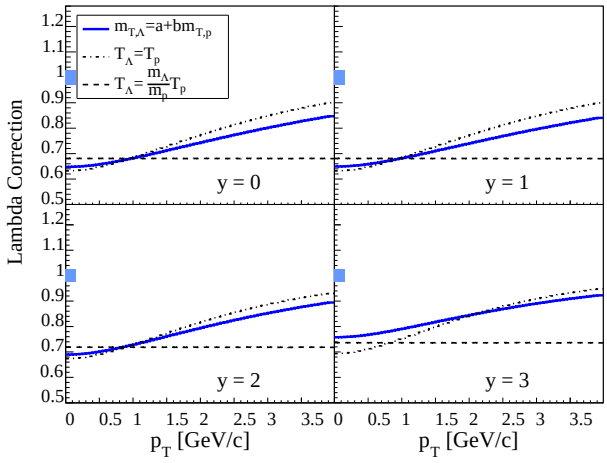

FIG. 2: (Color online) The p_T dependent feed-down correction factors for protons versus $p_T$and rapidity. The 3 sets of lines show the effect of various scenarios for the difference in shape between proton the and Λ spectra. Systematic errors on the correction due to uncertainties in the yield ratio of protons and lambdas are shown by the bands to the left of the plots. The curves for anti-protons are very similar.

D. Feed-down corrections

We have corrected our data to account for the hyperons that decay into protons using the method described in [32]. The correction factor, C, is given by:

$$C = \frac{N_p}{N_p + N_\Lambda + N_{\Sigma^+}}, \tag{10}$$

where N_p is the number of primary protons and N_Λ and and N_{Σ^+} are the number of protons coming from Λ and Σ^+ decay respectively. Near central rapidity we have used the lambda spectra measured by PHENIX [35] and estimated the Σ/Λ ratio from lower energy measurements [33]. Since there are no measurements of Λs at forward rapidities we have estimated the Λ/p ratio based on thermal models that were fitted to the rapidity densities of charged pions, kaons, protons and anti-protons measured by BRAHMS in the forward region [34].

We find that $\frac{dN_\Lambda}{dy}/\frac{dN_p}{dy}$ varies only slowly in the model with rapidity up to rapidities $y \approx 4$. The systematic error from uncertainties on the yields and the model extrapolation is estimated to be less than 3%. The correction factor also depends on the p_T dependence of the Λ/p ratio. BRAHMS has found that the mean transverse kinetic energy scales linearly with the mass of the particle with a slope that depends only weakly on rapidity [36]. We have used these systematics to estimate the inverse slope (T) of the Λ m_T-distribution. To estimate the systematic error on the p_T dependence of the correction factor we have taken the limiting cases of $T_\Lambda = T_p$ and $T_\Lambda = T_p m_\Lambda/m_p$. This produces an error on the correction factor that is almost zero at $p_T = 1$ GeV/c and reaches -9%, +6% at $p_T = 2$ GeV/c. The correction factor as a function of p_T and rapidity is shown in Fig. 2. It varies only weakly with rapidity and has a systematic error that is small in comparison to the statistical errors on B_2 and the space averaged phase-space density. At $p_T = 2$ GeV/c the total error from the feed-down correction reaches a value of 19% for B_2 and 10% for the space averaged phase-space density.

III. RESULTS

Figure 3 shows our invariant proton and deuteron spectra versus p_T for the four measured rapidity bins. We fit exponentials in m_T to the spectra and extract the invariant yields, dN/dy and inverse slopes T. These are listed in Table I. The yields, of p, d, $\bar{p}$ and $\bar{d}$ fall steadily from y=0 to y=3. The inverse slopes of particles and antiparticles are very similar but those of the (anti)-deuterons are about 15% higher than those of the (anti)-protons. For the protons and anti-protons the inverse slopes decreases steadily with rapidity but we lack sufficient statistics to see a rapidity dependence in the deuteron slopes.

Figure 4 shows B_2 versus p_T and rapidity. B_2 increases with p_T, which is consistent with previous experiments [19, 21]. Using Eq. 2, we find that at central rapidity the source radius R_G falls from 4.6 ± 0.2 fm to 3.0 ± 0.4 fm as m_T increase from 0.7 to 2.0 GeV. This is consistent with the m_T dependence of HBT radii, $R \propto 1/\sqrt{m_T}$ that has been observed by PHENIX and STAR [22] and also at SPS energies, [18]. The solid line in each rapidity panel represents an exponential fit to our data at y=0. We see no evidence of any rapidity dependence of $B_2(p_T)$. The proton and anti-proton B_2 values are very close at this energy implying a similar source size. This is in contrast

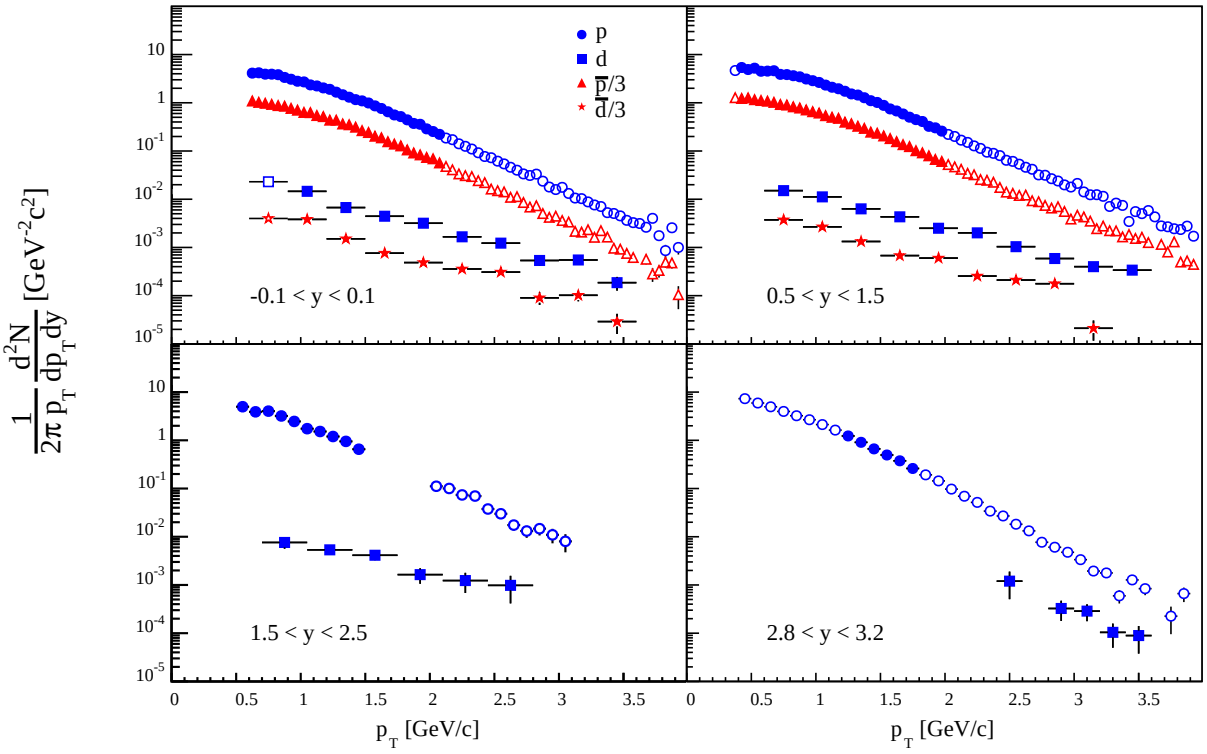

FIG. 3: (color online). (Anti)-proton and (anti)-deuteron p_T spectra at various rapidities. The filled symbol part of the spectra show the p_T intervals used in the coalescence analysis. Note the limits for the deuteron range are exactly twice those used for the protons.

	Proton			Deuteron		
y	p_T fit	dN/dy	T MeV	p_T fit	dN/dy	T MeV
0.0	0.7-4.0	27.9 ± 0.1	354 ± 2	0.7-3.3	0.136 ± 0.007	423 ± 23
		20.8 ± 0.1	352 ± 1		0.081 ± 0.005	404 ± 29
0.8	0.5-4.0	26.0 ± 0.1	356 ± 1	0.7-3.5	0.117 ± 0.003	463 ± 14
		17.9 ± 0.1	361 ± 1		0.071 ± 0.003	403 ± 20
2.0	0.5-3.0	20.9 ± 0.2	314 ± 3	0.8-2.8	0.082 ± 0.011	460 ± 110
3.1	0.5-4.0	23.4 ± 0.1	282 ± 1	2.5-3.5	$0.25^{+0.30}_{-0.08}$	310 ± 90

TABLE I: Inverse slopes, T (MeV), and dN/dy derived from fitting spectra. The lower row at rapidities $y = 0$ and $y = 0.75$ is for the anti-particles. Errors are statistical only.

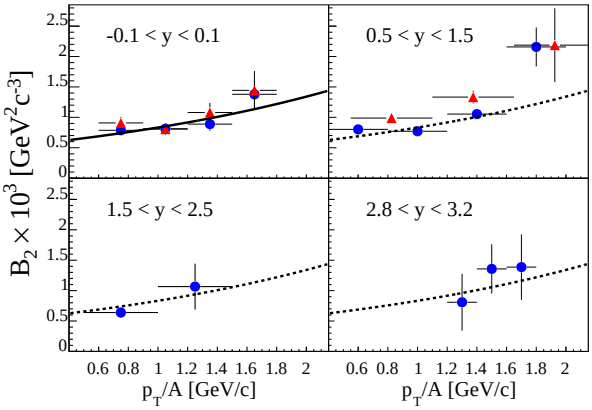

FIG. 4: (color online). B_2 versus transverse momentum per nucleon at several rapidities for central Au+Au collisions at $\sqrt{s_{\rm NN}}$ = 200 GeV. The solid line in the top left panel is an exponential fit to the data at y=0. This same line is shown, in dotted form, in the other 3 panels.

to $\sqrt{s_{\rm NN}} = 17.3$ GeV where the anti-proton source volume was found to be somewhat larger than the proton source [16].

Figure 5 shows the average phase-space density $\langle f \rangle (m_T)$ for protons and anti-protons as a function of rapidity. The space averaged phase-space density decreases as the m_T increases as expected from Eq. 5. The solid curve in each panel of Fig. 5 is a exponential fit to the proton density at y=0. We see little rapidity dependence of $\langle f \rangle (p_T)$. By fitting the proton and anti-proton phase densities we find $\mu = 35 \pm 5$ MeV to be compared to the value of 22 MeV extracted with statistical models [37]. Near y=0 the anti-protons have a slightly smaller value of space averaged phase-space density compared to that of protons. At $\sqrt{s_{\rm NN}} = 17.3$ GeV the anti-proton space averaged phase-space density was 38 times smaller [16] suggesting a much larger baryon chemical potential at the

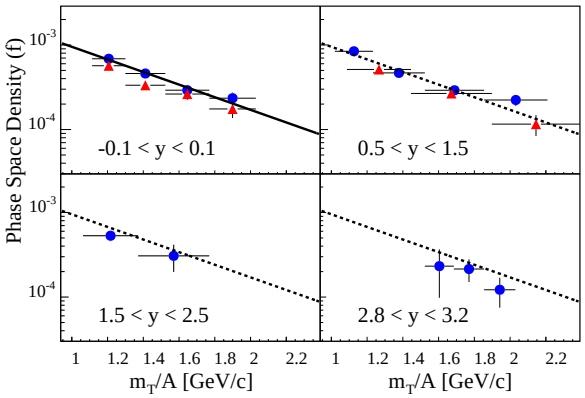

FIG. 5: (color online). The (anti)-proton space averaged phase-space density $\langle f \rangle (m_T/A)$ for central $\sqrt{s_{\rm NN}}$ = 200 GeV Au+Au collisions at several rapidities. The solid line in the top left panel is an exponential fit to the data at y=0. This same line is shown, in dotted form, in the other 3 panels.

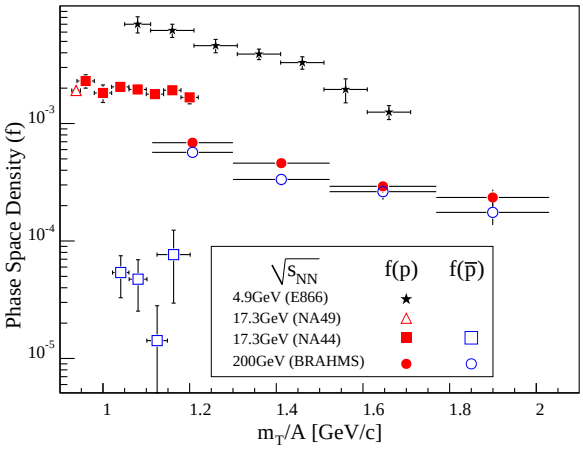

FIG. 6: (color online). The proton space averaged phase-space density as a function of $\sqrt{s_{\rm NN}}$ and m_T at y=0, [8, 16, 19, 38]

lower energy. The inverse slope derived from the space averaged phase-space density is $T = 610 \pm 40$ MeV. This is consistent with data at $\sqrt{s_{\rm NN}}$ = 17.3 GeV but much higher than at $\sqrt{s_{\rm NN}}$ = 4.9 GeV where the inverse slope is about 350 MeV, see Fig. 6. It should be noted that the proton, kaon and pion spectra can be well described by blast wave fits, which suggest that this increase in the inverse slope is largely driven by an increase in radial flow. This is supported by the fact that the phase density of pions is characterized by a much smaller inverse slope ($\approx$ 140 MeV) than that of protons [16].

Figures 4 and 5 imply that the volume of homogeneity, $1/B_2$, and the space averaged phase-space density vary little with rapidity at $\sqrt{s_{\rm NN}}$ = 200 GeV. This is in stark contrast to the situation at lower energy. Table II shows the rapidity dependence of B_2 and the space averaged phase-space density at $p_T = 0$ for central Pb+Pb collisions at $\sqrt{s_{\rm NN}}$ = 17.3 GeV [9, 16, 38]. These data are compared to BRAHMS results at p_T/A = 1.3 GeV/c which show very little rapidity dependence. Finally, Fig. 6 shows the evolution of the space averaged phase-space density near mid-rapidity as the energy of the system grows from AGS to RHIC values. The space averaged phase-space density of protons decreases with energy while that of anti-protons increases.

$(p_T/A = 0)$	y=0.2	y=0.8	y=1.3
$B_2 \times 10^4$	7.9 ± 0.8	8.1 ± 0.3	13.7 ± 2.7
$f \times 10^3$	1.9 ± 0.1	2.5 ± 0.2	3.3 ± 0.3

$(p_T/A$ =1.3 GeV/c)	y=0.0	y=1.0	y=2.0	y=3.1
$B_2 \times 10^4$	8.8 ± 1.0	10.0 ± 0.7	10.6 ± 0.4	8.1 ± 0.5
$f \times 10^3$	2.9 ± 0.4	2.9 ± 0.2	3.1 ± 1.0	2.3 ± 1.0

TABLE II: (color online). The rapidity dependence of B_2 and the f for (Top) Pb+Pb collisions at $\sqrt{s_{\rm NN}}$= 17.3 GeV and (Bottom) $\sqrt{s_{\rm NN}}$ = 200 GeV AuAu collisions. For the 17.3 GeV data the centrality is 23% for at y=0.2 [38] and 20% at y=0.8 and 1.3 [9, 16].

IV. SUMMARY

Near central rapidity the proton and anti-proton phase space densities are very similar, suggesting a small baryon chemical potential. The coalescence parameters for deuterons and anti-deuterons are also very close, suggesting similar freeze-out volumes for protons and anti-protons. This similarity is less clear at lower energies. B_2 increases with p_T as expected for a system undergoing transverse flow. Flow introduces a correlation between position and momentum that gets stronger as p_T increases. At a given p_T the coalescence parameter is independent of rapidity, which implies that the the volume of homogeneity for protons is almost constant from y=0 to y=3.1. It is interesting to note that the radial flow at a given p_T vary weakly with rapidity [36]. The weak dependence of radial flow on rapidity offers an explanation of why the p_T dependence of B_2 does not depend upon rapidity. It does not however address fact that the overall magnitude of B_2 is constant from y=0 to y=3.1. The proton space averaged phase-space density also shows no significant rapidity dependence, while depending strongly on m_T and $\sqrt{s_{\rm NN}}$. The number of protons per unity rapidity only decreases by a factor of 0.84 ± 0.01 from y=0 to y=3.1. The space averaged phase-space density can be thought of as the number of protons per unit volume. If the density is constant and the number of protons varies only slowly with rapidity, it is not surprising that the volume ($\approx 1/B_2$) varies little with rapidity. Despite a large drop in the multiplicity of produced particles from central

to forward rapidity the proton space average phase-space density varies little over three units of rapidity.

V. ACKNOWLEDGEMENTS

This work was supported by the Division of Nuclear Physics of the Office of Science of the U.S. Department of Energy under contracts DE–AC02–98–CH10886, DE–FG03–93–ER40773, DE–FG03–96–ER40981, and DE–FG02–99–ER41121, the Danish Natural Science Research Council, the Research Council of Norway, the Polish Ministry of Science and Information Society Technologies(Grant no. 1248/B/H03/2009/36), and the Romanian Ministry of Education and Research (5003/1999, 6077/2000). We thank the staff of the Collider-Accelerator Division at BNL for their excellent and dedicated work to deploy RHIC and their support to the experiment.

References

[1] S. Butler and C. Pearson, Phys. Rev. **129**, 836 (1963).
[2] J. Kapusta, Phys. Rev. **C21**, 1301 (1980).
[3] A.Z. Mekjian, Phys. Rev. **C17**, 1051 (1978)., Nucl. Phys. **A312**, 491 (1978).
[4] T.A. Armstrong, *et al.*, [E864 Collaboration] Phys. Rev. **C60** 064903 (1999).
[5] H. Gutbrod *et al.*, Phys. Rev. Lett. **37** 667 (1976); S. Nagamiya, M. C. Lemaire, E. Moeller, S. Schnetzer, G. Shapiro, H. Steiner, and I. Tanihata, Phys. Rev. **C24** 971 (1981); B. V. Jacak, D. Fox, and G. D. Westfall *ibid.* **31** 704 (1985); J.W. Cronin *et al.*, Phys. Rev. **D11**, 3105 (1975).
[6] S. Afanasiev *et al.* [PHENIX Collaboration], Phys. Rev. Lett. **99**, 052301 (2007)
[7] B. I. Abelev *et al.* [STAR Collaboration], arXiv:0909.0566 [nucl-ex].
[8] L. Ahle *et al.* [E866 Collaboration], Phys. Rev. **C60**, 064901 (1999), L. Ahle *et al.* [E866 Collaboration] Phys. Rev. **C57**, R466 (1998).
[9] I. G. Bearden *et al.* [NA44 Collaboration], Eur. Phys. J. **C23**, 237-247 (2002).
[10] S. S. Adler *et al.* [PHENIX Collaboration], Phys. Rev. Lett. **94**, 122302 (2005).
[11] S. Das Gupta and A. Z. Mekjian, Phys. Rep. **72**, 131-183, (1981).
[12] H. Sato and K. Yazaki, Phys. Lett. **B98**, 153, (1981).
[13] Rüdiger Scheibl and Ulrich Heinz, Phys. Rev. **C59**, 1585 (1999),
[14] W. J. Llope et al., Phys. Rev. **C52**, 2004 (1995).
[15] P. E. Hodgson, Nuclear Reactions and Nuclear Structure Clarendon-Press, Oxford, p453, (1971).
[16] M. Murray and B. Holzer, Phys. Rev. **C63**, 054901 (2001).
[17] H. Bøggild *et al.* [NA44 Collaboration Phys. Lett. **B458**, 181 (1999).
[18] H. Beker *et al.*, [NA44 Collaboration], Phys. Rev. Lett. **74**, 3340 (1995).
[19] I. G. Bearden *et al.* [NA44 Collaboration], Phys. Rev. Lett. **85**, 2681 - 2684 (2000).
[20] C. Adler *et al.* [STAR Collaboration], Phys. Rev. Lett. **87**, 262301, (2001).
[21] S. S. Adler *et al.* [PHENIX Collaboration], Phys. Rev. Lett. **94**, 122302 (2005).
[22] J. Adams *et al.* [STAR Collaboration], Phys. Rev. **C71**, 044906 (2005).
[23] Y. Oh, Z. W. Lin and C. M. Ko, Phys. Rev. **C80**, 064902 (2009) [arXiv:0910.1977 [nucl-th]].
[24] B. Tomasik and U. W. Heinz, Phys. Rev. **C65**, 031902 (2002)
[25] M. J. Murray, J. Phys. **G28**, 2069 (2002)
[26] G. F. Bertsch, Phys. Rev. Lett. **72**, 2349 (1994) [Erratum-ibid. **77**, 789 (1996)]
[27] S. Pal and S. Pratt, Phys. Lett. **B578**, 310 (2004)
[28] R. Debbe *et al.*, Nucl. Inst. Meth. **A570**, 216, (2007).
[29] M. Adamczyk *et al.* [BRAHMS Collaboration], Nucl. Inst. Meth. **A499**, Issues 2-3, 437, (2003).
[30] I. Arsene *et al.* [BRAHMS Collaboration], Phys. Rev. **C72**, 014908, (2005).
[31] GEANT CERN Program Library.
[32] I. G. Bearden *et al.* [BRAHMS Collaboration], Phys. Rev. Lett. **93**, 102301, (2004).
[33] H. Sorge, Phys. Rev. **C52**, 3291 (1995).
[34] L. A. Stiles and M. Murray, arXiv:nucl-ex/0601039.
[35] K. Adcox *et al.* [PHENIX Collaboration], Phys. Rev. Lett. **89**, 092302 (2002).
[36] S. J. Sanders *et al.* , arXiv:nucl-ex/0907.4741v1.
[37] A. Andronic, P. Braun-Munzinger, J. Stachel Nucl.Phys. **A772**, 167-199, (2006).
[38] T. Anticic *et al.* [NA49 Collaboration], Phys. Rev. **C69**, 024902 (2004).